Randomly arranged cation-ordered nanoregions in lead-free relaxor ferroelectric K$_{1/2}$Bi$_{1/2}$TiO$_3$: Prediction from first-principles study

Manish K. Niranjan, P. Karuna Kumari, Krishnarjun Banerjee, and Saket Asthana

Articles you may be interested in

CrossMark
click for updates

Randomly arranged cation-ordered nanoregions in lead-free relaxor ferroelectric $K_{1/2}Bi_{1/2}TiO_3$: Prediction from first-principles study

Manish K. Niranjan,[a)] P. Karuna Kumari, Krishnarjun Banerjee, and Saket Asthana
Department of Physics and Advanced Functional Materials Laboratory, Indian Institute of Technology, Hyderabad, TS, 502285, India

First-principles density functional calculations are performed to investigate the lattice dynamics, Infrared reflectivity, and Raman intensity spectra of a lead-free ferroelectric $K_{1/2}Bi_{1/2}TiO_3$ system. In particular, the A-site cation ordering in $K_{1/2}Bi_{1/2}TiO_3$ and its effects on lattice dynamics and the Raman spectrum are explored. The results suggest that the cation ordering at the A-site in $K_{1/2}Bi_{1/2}TiO_3$ significantly influences its Raman spectra. From the analysis of theoretical and experimental Raman spectra, it is suggested that randomly arranged cation ordered nanoregions with different A-site orderings are formed in $K_{1/2}Bi_{1/2}TiO_3$ samples. The random arrangement is favored by entropy contributions to free energy and may explain the lack of observed long-range A-site cation ordering in $K_{1/2}Bi_{1/2}TiO_3$. Further, it is suggested that partial A-site cation ordering may also occur in $K_{1/2}Bi_{1/2}TiO_3$ favored by kinetic factors during sample preparation. The Born effective charges of K and Bi ions at the A-site are computed and found to be significantly disparate, thereby suggesting hetero-polar activity at the A-site in $K_{1/2}Bi_{1/2}TiO_3$. The formation of A-site hetero-polar cation ordered nanoregions and their random or/and partially ordered arrangement in $K_{1/2}Bi_{1/2}TiO_3$ may play an important role in the determination of its relaxor properties apart from the dominant role played by polar nanoregions. The computed Infrared reflectivity and Raman intensity spectra are expected to provide benchmark first-principles results for further analysis of experimental spectra and results. *Published by AIP Publishing.*
https://doi.org/10.1063/1.5021410

I. INTRODUCTION

Complex oxides exhibit fascinating structures and physical properties which make them highly promising for a variety of technological applications. In particular, lead-based oxides such as $Pb(Zr_{1-x}Ti_x)O_3$ (PZT) and related compositions have been widely used as primary functional materials in high-performance sensors, actuators, and transducers for many years.[1,2] PZT and related compositions near the morphotropic phase boundaries (MPBs) are particularly advantageous for electromechanical device applications due to their superior dielectric and piezoelectric properties. However, lead-based PZT and related materials also pose serious health and environmental risks due hazardous nature of lead. This has led to an enormous push in the last two decades towards the development of lead-free and environmentally friendly high performance piezoceramics.[3–5] In recent years, bismuth (Bi) containing perovskite oxides such as $K_{1/2}Bi_{1/2}TiO_3$ (KBT), $Na_{1/2}Bi_{1/2}TiO_3$ (NBT), and their solid solutions have emerged as promising alternative materials that may be developed as high performance lead-free piezoceramics.[6–10] The piezoelectric and dielectric properties in these oxides comparable to those for PZT are indeed expected due to the presence of the bismuth cation (Bi^{3+}). The Bi^{3+} ion contains a $6s^2$ lone electron pair which is known to play a critical role in driving ferro- and piezoelectric properties in lead-based ceramics. $K_{1/2}Bi_{1/2}TiO_3$ is an excellent relaxor ferroelectric

that exhibits a broad dielectric peak at the frequency-dependent dielectric maximum temperature of $T_m \sim 380°$ C.[9,11,12] It undergoes phase transformation with the structure changing from cubic ($Pm3$-m) to pseudocubic at $T_C \sim 410°C$ and from pseudocubic to tetragonal ($P4mm$) at a temperature of $\sim 270°C$.[13] Pure $K_{1/2}Bi_{1/2}TiO_3$ exhibits moderate dielectric and piezoelectric properties ($\varepsilon_r \approx 770$, $d_{33} \approx 80$–100 pC/N, and $S_{max}/E_{max} \approx 130$ pm/V).[3] Nevertheless, improved piezoelectric properties have been achieved in $K_{1/2}Bi_{1/2}TiO_3$ based solid solutions as well as in $K_{1/2}Bi_{1/2}TiO_3$ with cations substituted at the A and B-sites. For over many years, the cation substitution in perovskite oxides has been successfully exploited to tailor physical properties and to introduce novel functionalities. In cation substituted perovskites, the arrangement of cations on different sublattices can vary from fully ordered to fully random. Furthermore, the degree of ordering can have significant and remarkable effects on various structure-property relations.[14] In general, the ordering of B-site cations in the ABO_3 type perovskite is more common than that of A-site cations. Cation ordering is driven by electrostatic considerations arising due to the difference in the radius and oxidation states (formal charge) of the cations. On the other hand, disorder is favored by configurational entropy in case the cation sizes and formal charges are similar. Thus, the ordered arrangement of cations is expected if the oxidation states of cations on A or B sites differ by more than two, whereas the disordered arrangement is expected if the difference is less than two. However, if the oxidation states of cations differ exactly by two, then the

a)E-mail: manish@iith.ac.in. Tel.: (91)040-23016092. Fax: (91)040-23016032.

arrangement may be fully disordered, partially ordered, or fully ordered depending on bonding preference or/and differences in the size of cations. In the case of $Na_{1/2}Bi_{1/2}TiO_3$, the Na^+ (1.32 Å) and Bi^{3+} (1.31 Å) cations on A-sites have similar ionic radii and have a relative charge difference of 2e. Therefore, the cation arrangement on the A-site sublattice is expected to be disordered. This is also in agreement with experimental and first-principles theoretical studies reported on $Na_{1/2}Bi_{1/2}TiO_3$.[15–17] On the other hand, in the case of $K_{1/2}Bi_{1/2}TiO_3$, the K^+ ion has an ionic radius of 1.65 Å which is much larger than the Bi^{3+} radius of 1.31 Å. Thus, the difference in ionic radii of A-site cations can be expected to provide the driving mechanism for cation ordering on the A-site sublattice in $K_{1/2}Bi_{1/2}TiO_3$.[14] However, no conclusive evidence of ionic ordering in $K_{1/2}Bi_{1/2}TiO_3$ has been reported so far.[9,18,19] $K_{1/2}Bi_{1/2}TiO_3$ and its solid solutions are also interesting for further investigations as origins of its various intrinsic properties and structure-property correlations have not been fully explored. Recently, based on X-ray absorption fine structure (XAFS) studies, it was reported that the local environment of Bi ions in $K_{1/2}Bi_{1/2}TiO_3$ is much more distorted than that determined earlier from conventional diffraction experiments.[19] For many years, various structural aspects in oxides such as local distortions and ionic configurations have been widely explored using Raman and Infrared (IR) spectroscopy. In particular, the presence of new phases or structural changes can be very effectively determined using Raman spectroscopy, even in systems which exhibit no long-range structural ordering.[20,21] Although several experimental studies of $K_{1/2}Bi_{1/2}TiO_3$ and its solid solutions have been reported due to its technological importance, reported theoretical studies of $K_{1/2}Bi_{1/2}TiO_3$ are scarce.[22,23] Further, though few experimental Raman spectroscopic studies of $K_{1/2}Bi_{1/2}TiO_3$ have been reported,[9,24,25] no experimental Infrared (IR) study of $K_{1/2}Bi_{1/2}TiO_3$ has been reported to the best of our knowledge. Moreover, no theoretical study of Infrared and Raman intensity spectra of $K_{1/2}Bi_{1/2}TiO_3$ has been reported. Theoretical studies of Raman and Infrared spectra of $K_{1/2}Bi_{1/2}TiO_3$ are important in that local environment and cation ordering configurations may be identified from the features of these spectra.

Here, we present a first-principles study of cation ordering and its effect on Raman intensity and Infrared reflectivity spectra in $K_{1/2}Bi_{1/2}TiO_3$ within the framework of density-functional theory. From the analysis of the theoretical Raman study and our recently reported experimental study,[25] it is suggested that the cation ordering in $K_{1/2}Bi_{1/2}TiO_3$ significantly influences the Raman spectra. Further, it is suggested that randomly arranged nanoscale size regions with different A-site orderings may be formed in $K_{1/2}Bi_{1/2}TiO_3$ samples. This randomness in arrangement may explain the lack of observation of long-range cation ordering despite the significant size difference of K^+ and Bi^{3+} ions on A-sites in $K_{1/2}Bi_{1/2}TiO_3$. The study also suggests that the variance in reported experimental Raman modes may be indicative of different partial A-site cation ordering in $K_{1/2}Bi_{1/2}TiO_3$ samples. The formation of A-site cation ordered nanoregions in $K_{1/2}Bi_{1/2}TiO_3$ may be considered qualitatively similar to compositionally ordered regions (CORs) formed in well-

known relaxor ferroelectrics of type $A(B'B'')O_3$ such as $Pb(Mg_{1/3}Nb_{2/3})O_3$.[26–28] Thus, in addition to polar nanoregions (PNRs), the cation ordered regions and their coupling to PNR in $K_{1/2}Bi_{1/2}TiO_3$ may also play a critical role in determination of its relaxor properties. Besides theoretical Raman and Infrared spectra, the local structure of $K_{1/2}Bi_{1/2}TiO_3$ and, in particular, Bi-O and Ti-O bond distances are computed and the results are compared with reported X-ray absorption fine structure (XAFS) spectroscopy results. Further, the spontaneous polarization, Born-effective charge tensors of ions, oscillator strengths, and effective charges of phonon modes are computed and various atomistic mechanisms relevant to physical properties of $K_{1/2}Bi_{1/2}TiO_3$ are determined.

The rest of the article is organized as follows. Theoretical details are presented in Sec. II. In Sec. II A, the computational methodology is presented. The structure and energies of A-site cation ordering configurations of $K_{1/2}Bi_{1/2}TiO_3$ are presented in Sec. II B. Calculations of phonon mode frequencies at Brillouin zone-center and Born effective charges are presented in Secs. II C and II D. Analyses of computed Infrared reflectivity and Raman intensity spectra are presented in Secs. II E and II F. Finally, conclusions are presented in Sec. III.

II. THEORETICAL DETAILS

A. Computational methodology

Density functional theoretical framework (DFT) is used to perform calculations within local density approximation (LDA) as implemented in PWscf package.[29] The core and valence electron interactions are approximated using the Troullier-Martins (TM) form of norm-conserving pseudopotential (NCPP).[30] A plane wave basis set with a kinetic energy cutoff of 100 Ry is used to expand the Kohn-Sham wavefunctions. Sampling of Brillouin zones of $1 \times 1 \times 2$ (10 atoms) and $2 \times 2 \times 2$ (40 atoms) $K_{1/2}Bi_{1/2}TiO_3$ unit cells is performed using $8 \times 8 \times 4$ and $4 \times 4 \times 4$ Monkhorst-Pack k-point meshes, respectively. Self-consistency in the calculations is achieved with total energies converging to 10^{-6} eV/cell. The ionic relaxations are performed until the largest force on each ion is reduced to less than 0.005 eV/Å. The DFT-Linear response scheme with iterative Green's function approach of density-functional perturbation theory is used to compute the zone-center (k = 0) phonon frequencies, Born-effective charge tensors, dielectric permittivity tensors, and linear optical susceptibility.[29]

B. Crystal structure and A-site cation ordering in $K_{1/2}Bi_{1/2}TiO_3$

At room temperature, $K_{1/2}Bi_{1/2}TiO_3$ crystallizes in the tetragonal structure with $P4mm$ space group symmetry. The reported experimental lattice parameters for tetragonal $K_{1/2}Bi_{1/2}TiO_3$ are $a = b = 3.913$ Å and $c = 3.990$ Å.[25,31] Figure 1 shows the computed total and projected density of electronic states for $K_{1/2}Bi_{1/2}TiO_3$. The width of the valence band (VB) is computed to be ~5.3 eV. The valence band is primarily composed of O-*2p* states. The O-*2p* and Bi-*6p* orbitals in the lower energy segment and O-*2p* and Ti-*3d*
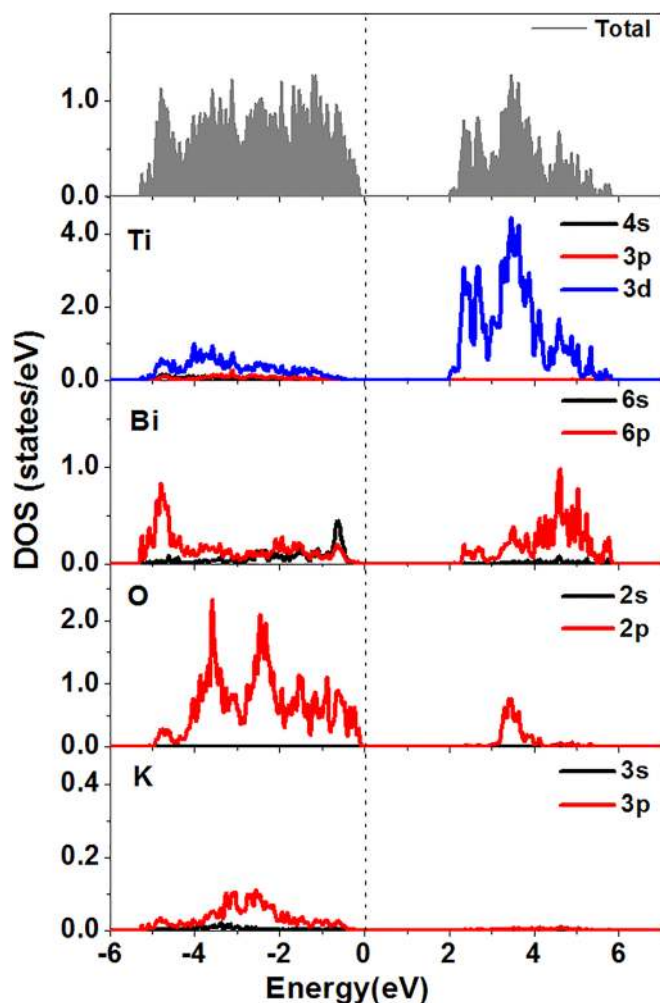
FIG. 1. (a) Total density of states in $K_{1/2}Bi_{1/2}TiO_3$. Partial density of states in $K_{1/2}Bi_{1/2}TiO_3$ projected onto orbitals of (a) Ti atom. (b) Bi atom, (c) O atom, and (d) K atom. Top of the valence band (VBM) is indicated by the dotted line at 0 eV.

orbitals in the higher energy segment of the VB are weakly hybridized resulting in mixed ionic-covalent bonding in $K_{1/2}Bi_{1/2}TiO_3$. The covalent-ionic type bonding between Bi and O atoms is also indicative of the lone pair effect similar to that of Pb^{2+} in PZT ceramics. The conduction band (CB) in the range of 2.0–5.8 eV is composed mainly of Ti-3d orbitals and some contribution from Bi-6p states.

Recently, using X-ray absorption fine structure (XAFS) spectroscopy, Shuvaeva *et al.*[19] reported the local environment of Bi and Ti atoms and, in particular, Bi-O and Bi-Ti distances in $K_{1/2}Bi_{1/2}TiO_3$. It was reported that the local environment of Bi is significantly distorted as compared to that determined from neutron diffraction data. The shortest Bi-O bond lengths of 2.22 Å were reported from the XAFS study which were shorter by 0.3 Å than those reported on the basis of crystallographic studies. In our study, the shortest Bi-O bond distance is computed to be 2.21 Å and thus is in good agreement with the experimental value obtained from the XAFS study. The short Bi-O distances indicate strong off-centering of Bi atoms in the oxygen polyhedral in $K_{1/2}Bi_{1/2}TiO_3$. The computed Bi-Ti distance is 3.22 Å which is also in good agreement with the reported value of 3.24 Å from the XAFS study.[19]

Next, we study A-site cation (Bi and K) ordering in $K_{1/2}Bi_{1/2}TiO_3$ by computing total energies of $2 \times 2 \times 2$ supercells of tetragonal $K_{1/2}Bi_{1/2}TiO_3$. Cation ordering at the A-site sublattice is simulated using $2 \times 2 \times 2$ tetragonal supercells containing 40 atoms. In the present study, the ionic positions in the supercells are relaxed while the lattice constants are kept fixed to experimental values ($a = b = 3.13$ Å; c/a = 1.021). Figure 2 shows different A-site ordering configurations in tetragonal $K_{1/2}Bi_{1/2}TiO_3$ supercells. The configurations are chosen and named following the works of Refs. 22 and 23. As can be seen in Fig. 2, the [001], [110], and [111] are layer, columnar, and rock-salt ordering configurations.[14] The energy is computed to be the lowest for the [001] or layered ordering configuration and the highest for the [111] or rock-salt configuration. The energies for different A-site ordering configurations relative to that of the [001] configuration are shown in Fig. 3. It may be noted that, in general, the layered ordered configuration is favored by A-site cations whereas rock salt ordering is favored by B-site cations.[14] The ordering configurations are favored by different oxygen anion environments around A- and B-site cations. As mentioned earlier, A-site cation ordering is expected in $K_{1/2}Bi_{1/2}TiO_3$ due to the sizeable difference in ionic radii of K^+ and Bi^{3+} ions. Further, cation ordering is expected if the difference in ionic charge is more than two whereas disordered arrangement is expected if the difference is less than two. Since the ionic charge of K^+ and Bi^{3+} cations differs by two, partially or fully ordered arrangement at the A-site is expected due to differences in the size of these cations. As can be seen in Fig. 3, the energy difference between different ordering configurations in tetragonal $K_{1/2}Bi_{1/2}TiO_3$ is less than 40 meV/f.u. Thus, no particular configuration is energetically favorable for long range A-site cation ordering. Nevertheless, nanoscale size regions or domains with random arrangement and with different A-site orderings may still be formed in $K_{1/2}Bi_{1/2}TiO_3$ as discussed further in Sec. II F. The randomness in ionic arrangement may explain as to why long-range A-site cation ordering has not been observed in $K_{1/2}Bi_{1/2}TiO_3$ though expected due to the significant difference in ionic radii of A-site cations.

C. Phonon frequencies at the Γ-point (k = 0)

The tetragonal unit cell of $K_{1/2}Bi_{1/2}TiO_3$ consists of ten atoms which gives rise to 27 optical phonon modes for wave-vector at the Brillouin zone center ($\mathbf{k} = 0$). Kriesel *et al.*[31] proposed symmetry classification of Raman-active, Infrared (IR)-active, and silent modes for $K_{1/2}Bi_{1/2}TiO_3$ with disorder at the A-sites as

$$\Gamma = \underbrace{3B_1 \oplus 2B_2}_{Raman} \oplus \underbrace{3A_1 \oplus 7E}_{Raman+IR} \oplus \underbrace{5A_2}_{Silent}. \quad (1)$$

The E modes are degenerate whereas A_1, A_2 and B_1, B_2 modes are non-degenerate. Computed frequencies of phonon modes and associated IR and Raman activities are shown in Table I and Fig. 4. It may be seen that modes with frequencies of 117, 278, 384, 468, and 589 cm^{-1} have negligible IR and Raman activities and thereby can be considered as silent
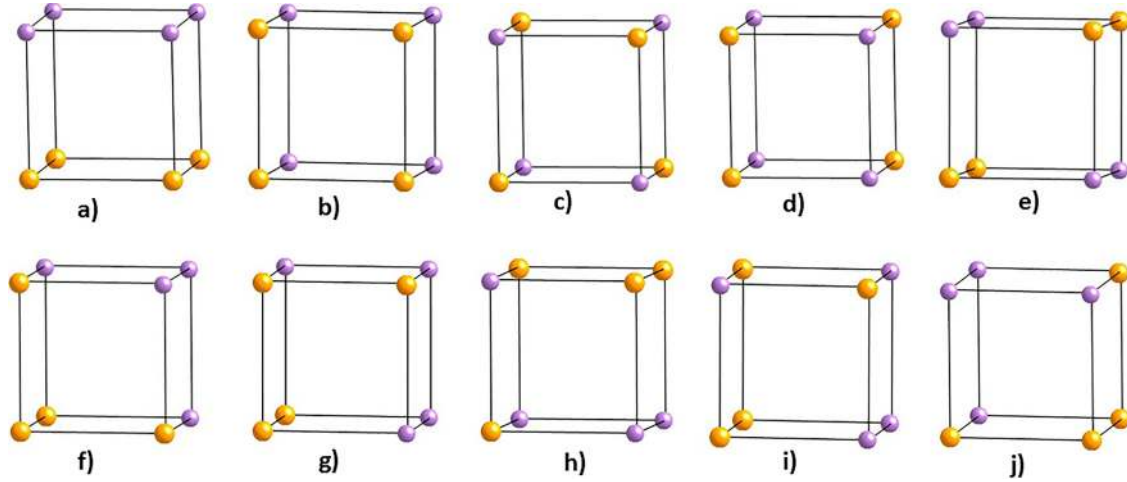
FIG. 2. A-site cation ordering configurations in $2 \times 2 \times 2$ tetragonal $K_{1/2}Bi_{1/2}TiO_3$ unit cells. Types of different orderings are (a) [001], (b) [100], (c) [111], (d) [110], (e) [011], (f) [all3 + 1], (g) [10–01$_z$], (h) [11–01$_{xy}$], (i) [11–10$_{xy}$], and (j) [00–01$_z$]. K and Bi atoms are indicated by yellow and purple balls. (Only A-site cations and sublattice are shown.)

modes. Table I also shows that degeneracy of expected E modes is lifted by a frequency of $\sim$3 cm^{-1} or less. These differences from the reported experimental results may be partially attributed to implicit A-site ordering in the $K_{1/2}Bi_{1/2}TiO_3$ tetragonal unit cell. The tetragonal unit cell of $K_{1/2}Bi_{1/2}TiO_3$ has the [001] or layer ordering configuration which is also the lowest energy configuration (see Sec. II B). As seen in Fig. 4, the mode frequencies form four major bands with the frequency range of 66–168 cm^{-1}, 218–285 cm^{-1}, 334–384 cm^{-1}, and 467–608 cm^{-1}. Recently, we had reported an experimental study of Raman spectra and other physical properties of $K_{1/2}Bi_{1/2}TiO_3$.[25] The computed and experimental Raman mode frequencies are shown and compared in Fig. 4.[9,24,25] As can be seen, the calculated mode frequencies are in reasonable agreement with experimental frequencies. It may be noted that theoretical mode frequencies correspond to zero temperature values whereas experimental values are obtained at room temperature. The mode frequencies are expected to be lowered by $\sim$3–4 cm^{-1} for temperature increment from 0 to 300 K due to anharmonic contributions

arising from thermal expansion and phonon–phonon coupling.[32] It may be noted that mode frequencies reported in different experimental works also show some degree of variance. For instance, mode frequencies of 345, 500, and 544 cm^{-1} were reported in Ref. 24 whereas 332 and 529 cm^{-1} were reported in Ref. 9. The mode frequencies of 345, 487, and 536 cm^{-1} were reported by us in Ref. 25. As
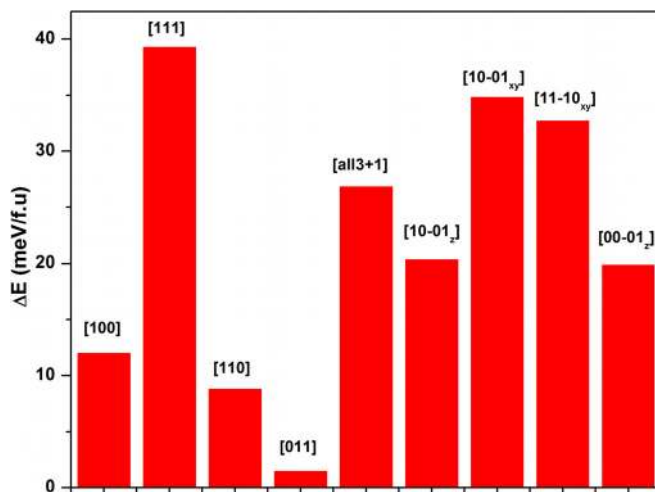

FIG. 3. Total energies of different ordering configurations (see Fig. 2) with respect to energy of the [001] or layered configuration. (Energy of the [001] configuration is set at 0.0 eV.)

TABLE I. Computed frequencies (cm^{-1}) of zone-center phonon modes, IR oscillator strength tensor coefficients ($\times 10^{-5} a.u$), mode effective charges and relative IR activity and relative Raman activity for tetragonal $K_{1/2}Bi_{1/2}TiO_3$.

| ν	S_{xx}	S_{yy}	S_{zz}	$Z^*_{m,x}$	$Z^*_{m,y}$	$Z^*_{m,z}$	IR act.	Raman Act.	I/I_{max}
66	0.0	22.7	0.0	0.0	−4.1	0.0	0.16	0.03	0.78
117	0.1	0.0	0.0	−0.3	−0.04	0.0	0.00	0.01	0.12
121	0.0	0.0	25.8	0.0	0.0	3.7	0.18	0.03	0.24
129	0.0	0.0	17.9	0.0	0.0	3.4	0.13	0.00	0.03
140	0.0	23.6	0.0	0.02	−3.7	0.0	0.17	0.01	0.09
143	0.0	0.0	0.04	0.0	0.0	0.1	0.00	0.02	0.15
166	0.0	0.0	25.1	0.0	0.0	3.3	0.18	0.01	0.06
168	8.0	0.0	0.0	−2.2	−0.01	0.0	0.06	0.03	0.14
218	0.0	0.0	143.3	0.0	0.0	8.8	1.00	0.08	0.26
230	0.0	60.6	0.0	0.01	−4.8	0.0	0.43	0.11	0.33
240	1.4	0.0	0.0	0.7	0.1	0.0	0.01	0.03	0.09
251	0.0	0.0	0.0	0.0	0.0	0.02	0.00	0.06	0.18
278	0.0	0.0	1.5	0.0	0.0	0.8	0.01	0.01	0.02
284	12.2	10.6	0.0	−2.2	2.0	0.0	0.16	0.05	0.11
285	1.35	107.1	0.0	0.7	6.4	0.0	0.77	0.06	0.14
335	63.1	0.0	0.0	−4.7	0.04	0.0	0.45	0.27	0.47
350	0.1	17.6	0.0	−0.2	2.3	0.0	0.13	0.00	0.00
355	101.1	0.0	0.0	5.9	0.1	0.0	0.71	0.62	1.00
369	0.0	0.0	40.0	0.0	0.0	−3.6	0.28	0.01	0.01
384	0.6	0.0	0.0	0.4	0.0	0.0	0.00	0.04	0.06
468	0.0	0.0	8.9	0.0	0.0	1.6	0.06	0.00	0.00
523	21.5	0.0	0.0	−3.0	−0.01	0.0	0.15	0.36	0.34
527	0.0	0.0	0.0	0.0	0.0	0.02	0.00	0.24	0.22
551	0.0	45.6	0.0	−0.02	−3.7	0.0	0.32	0.06	0.06
589	0.0	0.0	2.6	0.0	0.0	−0.9	0.02	0.03	0.03
608	125.1	0.0	0.0	6.2	−0.01	0.0	0.88	1.00	0.77
732	0.0	0.0	70.1	0.0	0.0	4.6	0.50	0.06	0.04
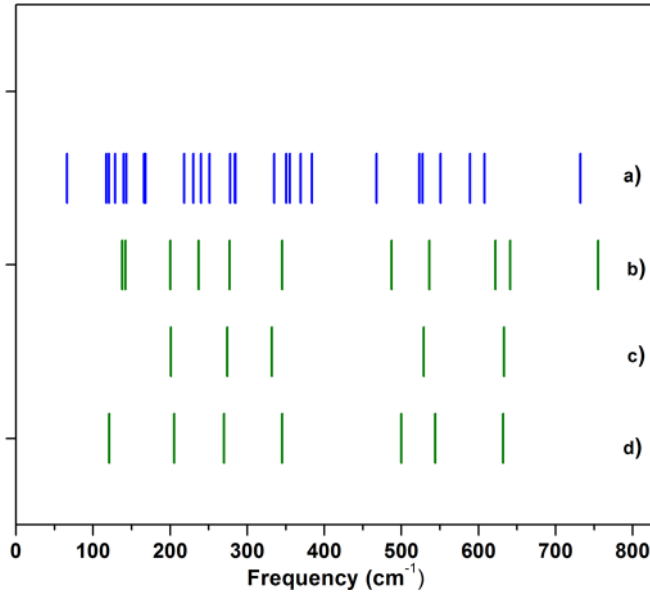
FIG. 4. Computed frequencies of (a) phonon modes of tetragonal $K_{1/2}Bi_{1/2}TiO_3$. Experimental frequencies of Raman-active modes (b) Ref. 25, (c) Ref. 9, and (d) Ref. 24.

discussed further in Sec. II F, the disparity in experimental mode frequencies may be indicative of different configurations of local A-site cation ordering in nanoregions of $K_{1/2}Bi_{1/2}TiO_3$. The lower frequency modes below $\sim 150\,cm^{-1}$ are primarily due to Bi ion vibrations whereas K-O and TiO_6 vibrations contribute to modes in the frequency band of $166-251\,cm^{-1}$ and $277-468\,cm^{-1}$, respectively. Oxygen ion vibrations contribute to higher frequency modes in the range of $523-732\,cm^{-1}$.

D. Born and mode effective charge tensors

The Born effective charge tensor component, $Z^*_{ij,\tau}$, of an atom τ is the measure of induced polarization along the ith direction caused by unit displacement of the τ atom sublattice in the jth direction. In general, the deviation of Born effective charge of an ion from its nominal charge is indicative of its off-centering which in turn is measure of its ferroactivity.[33] Table II presents the computed effective charge tensor components of cations (K, Bi, and Ti) and anions (O). Z* tensor of K, Bi, and Ti cations is almost diagonal due to higher local site

symmetries. However, O has lower local site symmetry and hence Z* of O ions is quite anisotropic with independent components. As can be seen in Table II, Z* of Bi, Ti, and O ions exhibits significant deviation from their nominal ionic charge values. This deviation is indicative of large covalent character in mixed ionic-covalent Bi-O and Ti-O bonding which results from hybridization of O-2p orbitals with Bi-6p and Ti-3d orbitals. In the case of the K ion, the deviation of Z* from its nominal ionic value of +1e is very small, which indicates that K-O bonding is primarily ionic in character. The Z* of the Bi atom has diagonal components of +3.58e, +5.05e, and +4.16e which are higher than the ionic value of +3e. Likewise, the Z* of two Ti atoms has diagonal components of +6.44e, +5.59e, and +6.16e which are higher than the ionic value of +4e. It is interesting to note that the Z* of the two Ti ions in $K_{1/2}Bi_{1/2}TiO_3$ is not disparate as compared to those reported for $Na_{1/2}Bi_{1/2}TiO_3$ in the *R3C* phase.[17] Thus, no hetero-ferroactive (or heteropolar) order or disorder is expected and relevant on the B-site Ti cations in $K_{1/2}Bi_{1/2}TiO_3$ similar to that proposed for $Na_{1/2}Bi_{1/2}TiO_3$. The diagonal components of Z^* tensor of O atoms vary from $-1.21e$ to $-6.51e$ deviating from the nominal ionic value of $-2e$. The mode effective charges ($Z^*_{m,\alpha}$) are also computed in order to assess effective charge associated with individual phonon modes.[34] The computed values of $Z^*_{m,\alpha}$ are presented in Table I. As can be seen, computed values of $Z^*_{m,\alpha}$ are significant for modes with frequencies of $218\,cm^{-1}$, $285\,cm^{-1}$, $355\,cm^{-1}$, and $608\,cm^{-1}$. The magnitude of $Z^*_{m,\alpha}$ for these modes is 8.8e, 6.4e, 5.9e, and 6.2e, respectively. Using the Berry phase method,[35] the spontaneous polarization (P_s) of $K_{1/2}Bi_{1/2}TiO_3$ is computed to be $42.9\,\mu C/cm^2$. The computed value of spontaneous polarization is in reasonable agreement with the reported experimental values which vary in the range of $22-49\,\mu C/cm^2$.[12,25,36,37]

E. Dielectric permittivity and infrared reflectivity spectrum

The frequency dependent complex dielectric permittivity tensor of a dielectric material can be expressed as[32,33]

$$\varepsilon_{\alpha\beta}(\omega) = \varepsilon^{\infty}_{\alpha\beta} + \sum_m \varepsilon_{m,\alpha\beta}(\omega)$$
$$= \varepsilon^{\infty}_{\alpha\beta} + \frac{4\pi}{\Omega} \sum_m \frac{S_{m,\alpha\beta}}{\omega^2_m - \omega^2 + i\gamma_m\omega}, \qquad (2)$$

TABLE II. Computed Born effective charge tensor components of K, Ba, Ti, and O ions in tetragonal $K_{1/2}Bi_{1/2}TiO_3$. The last three columns show the eigenvalues of the symmetric part of the full tensor.

	Z^*_{xx}	Z^*_{xy}	Z^*_{xz}	Z^*_{yx}	Z^*_{yy}	Z^*_{yz}	Z^*_{zx}	Z^*_{zy}	Z^*_{zz}	Z^*_1	Z^*_2	Z^*_3
K	1.00	0.00	0.00	0.00	1.04	0.00	0.00	0.00	1.20	1.00	1.04	1.20
Bi	3.58	0.00	0.00	0.00	5.05	0.00	0.00	0.00	4.16	3.58	4.16	5.05
Ti1	6.44	0.00	−0.16	0.00	5.59	0.00	0.40	0.00	6.16	6.48	5.59	6.12
Ti2	6.44	0.00	0.16	0.00	5.59	0.00	−0.40	0.00	6.16	6.48	5.59	6.12
O1	−1.31	0.00	0.00	0.00	−1.20	0.00	0.00	0.00	−6.51	−1.31	−1.20	−6.51
O2	−1.91	0.00	0.00	0.00	−3.43	0.00	0.00	0.00	−3.25	−1.91	−3.43	−3.25
O3	−5.26	0.00	−0.39	0.00	−1.78	0.00	−0.55	0.00	−1.78	−5.32	−1.78	−1.72
O4	−5.26	0.00	0.39	0.00	−1.78	0.00	0.55	0.00	−1.78	−5.32	−1.78	−1.72
O5	−1.86	0.00	0.54	0.00	−4.54	0.00	0.58	0.00	−2.18	−1.44	−4.54	−2.60
O6	−1.86	0.00	−0.54	0.00	−4.54	0.00	−0.58	0.00	−2.18	−1.44	−4.54	−2.60

where $\varepsilon_{\alpha\beta}^{\infty}$ is the electronic dielectric permittivity tensor. $\varepsilon_{\alpha\beta}^{m}$ is the contribution of the mth mode to the dielectric permittivity. $S_{m,\alpha\beta}$, ω_m, and γ_m are the oscillator-strength, angular frequency, and damping coefficient for the mth optical phonon mode. Ω is the volume of the primitive cell. The oscillator strengths ($S_{m,\alpha\beta}$) are obtained from Born effective charge tensors ($Z_{\tau,\alpha\beta}^{*}$) (see Sec. II D) and the eigendisplacements ($U_m(\tau\beta)$) as[33]

$$S_{m,\alpha\beta} = \left(\sum_{\tau\alpha'} Z_{\tau,\alpha\alpha'}^{*} U_m^{*}(\tau\alpha')\right)\left(\sum_{\tau'\beta'} Z_{\tau',\beta\beta'}^{*} U_m^{*}(\tau'\beta')\right). \quad (3)$$

The eigen-displacements satisfy the normalizing condition which is expressed as

$$\sum_{\tau\beta} M_\tau U_m^{*}(\tau\beta) U_n(\tau\beta) = \delta_{mn}, \quad (4)$$

where M_τ is the mass of ion τ.

The Infrared reflectivity of optical radiation normal to the surface is given as[33]

$$R = \left|\frac{\sqrt{\varepsilon_{\hat{q}}(\omega)} - 1}{\sqrt{\varepsilon_{\hat{q}}(\omega)} + 1}\right|^2, \quad (5)$$

where the dielectric permittivity function along the direction $\hat{q}$ is given as

$$\varepsilon_{\hat{q}}(\omega) = \sum_{\alpha\beta} \hat{q}_\alpha \varepsilon_{\alpha\beta}(\omega) \hat{q}_\beta.$$

The computed oscillator strengths of phonon modes for $K_{1/2}Bi_{1/2}TiO_3$ are shown in Table I. As can be seen, the oscillator strengths are significant for modes with frequencies of 218, 230, 285, 335, 355, 551, 608, and 732 cm^{-1}. The diagonal components and the average values of ε^{∞} and ε^0 are shown in Table III. The average values of ε^{∞} and ε^0 are computed to be 5.8 and 51.7 which are obtained by taking one-third of the trace of respective dielectric tensors. The LDA computed values of ε^{∞} components are expected to be overestimated by $\sim$10%. This is due to underestimated values of bandgaps and thus screening due to the lack of polarization dependence in the exchange-correlation functional.[38,39] Nevertheless, accuracy achieved in LDA computed values of several quantities which may critically depend on dielectric screening is much better than that for ε^{∞}.[40] Next, the real and imaginary parts of complex dielectric permittivity as a function of frequency in the range of 0–800 cm^{-1} are calculated using a damping constant of $\sim$10 cm^{-1} for all modes. As can be seen in Fig. 5, the absorption peaks are centered at modes having significant oscillator strengths (see Table I).
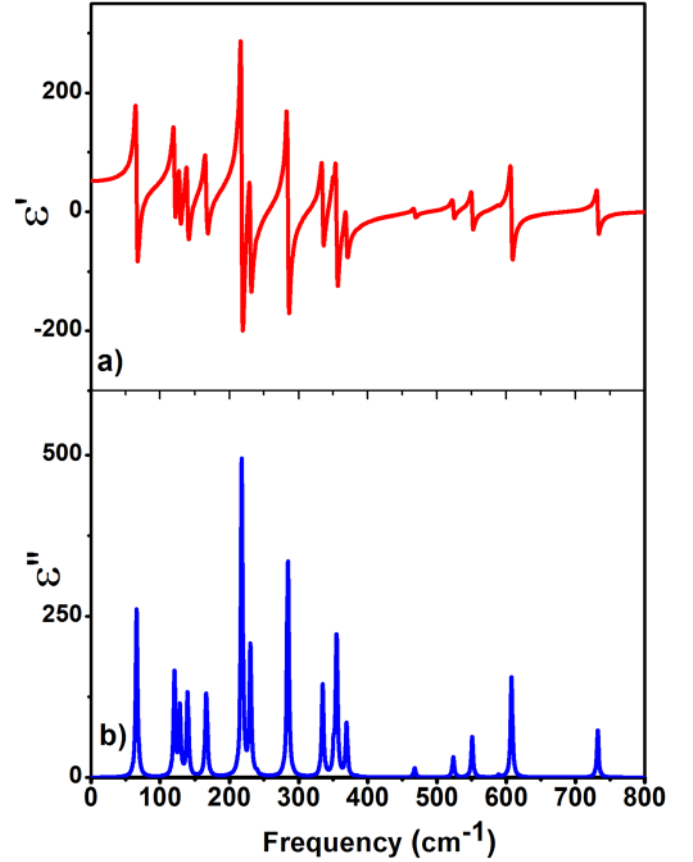

FIG. 5. Computed (a) real and (b) imaginary parts of dielectric permittivity as a function of frequency for tetragonal $K_{1/2}Bi_{1/2}TiO_3$.

The strong absorption peaks are centered at $\sim$218 cm^{-1}, 284 cm^{-1}, 334 cm^{-1}, 354 cm^{-1}, and 607 cm^{-1}. Figure 6 shows the IR reflectivity spectra for $K_{1/2}Bi_{1/2}TiO_3$ calculated using Eq. (5). The average reflectivity spectrum is shown in Fig. 6(a), whereas Figs. 6(b)–6(d) show the IR spectra at normal incidence on [100], [010], and [100] surfaces of single crystal $K_{1/2}Bi_{1/2}TiO_3$. The shape of the spectrum originates from the selective absorption at mode frequencies. At $\sim$342 cm^{-1}, the IR reflectivity decreases sharply for [100] and [010] surfaces, whereas it reduces to zero for the [001] surface. At $\sim$500 cm^{-1}, the reflectivity reduces to zero for the [010] surface and attains the maximum for [001] incidence. The reflectivity increases and then reduces to zero at $\sim$530 cm^{-1} for the [100] surface. Further, at $\sim$610 cm^{-1}, the reflectivity is reduced to zero for the [001] surface and attains the maximum for [100] and [010] surfaces. The experimental IR spectra for tetragonal $K_{1/2}Bi_{1/2}TiO_3$ have not been reported to the best of our knowledge. Although the computed IR spectra of $K_{1/2}Bi_{1/2}TiO_3$ are expected to be in reasonable agreement with experimental spectra, some disagreement may nevertheless be expected. In our calculations, the mode independent damping factor is used to calculate IR spectra shown in Fig. 6. However, the damping factors may vary with mode frequencies, and in particular, the variation may be significant for low frequency modes.[32] Furthermore, the experimental IR spectrum may lack features contributed by modes with low oscillator strengths.[41] Additionally, the modes which are heavily damped and close in frequency may not be resolved

TABLE III. Computed electronic and static dielectric tensors of tetragonal $K_{1/2}Bi_{1/2}TiO_3$.

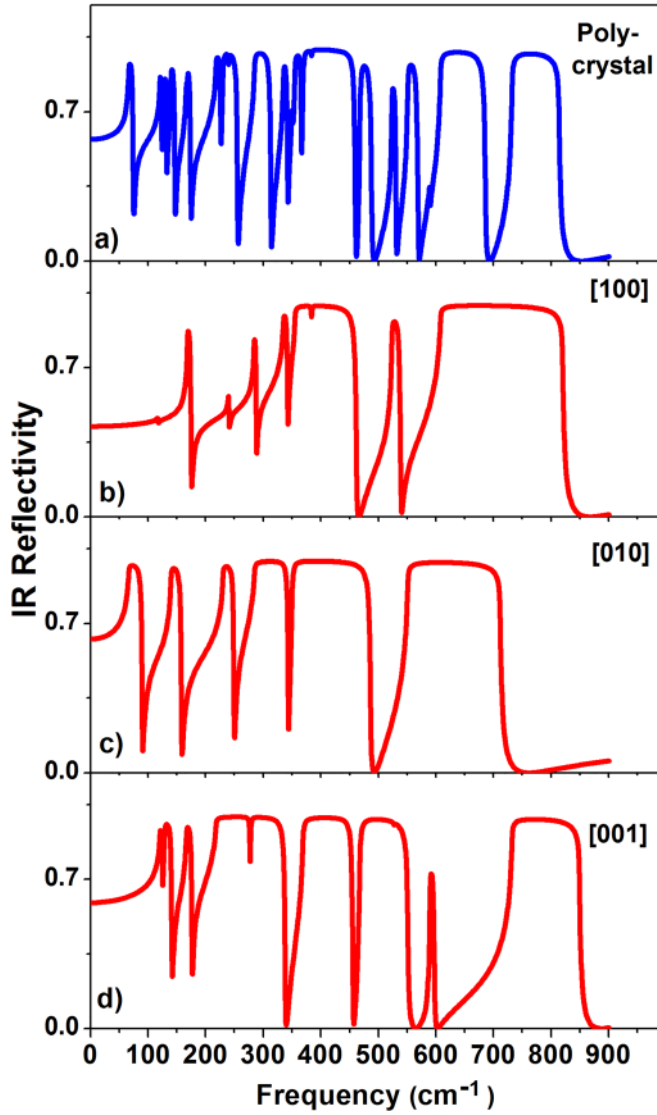|	ε^{∞}	ε_x^{∞}	ε_y^{∞}	ε_z^{∞}	ε^0	ε_x^0	ε_y^0	ε_z^0
Theory	5.75	5.87	5.66	5.73	51.69	22.50	73.93	58.64
Exp.	…	…	…	…	…	…	…	…

FIG. 6. Computed IR reflectivity spectra for (a) polycrystal (b)–(d) single crystal tetragonal $K_{1/2}Bi_{1/2}TiO_3$.

unambiguously. Thus, in general, only a few modes are required to fit the experimental IR spectrum.

F. Raman intensity spectrum

Raman scattering in crystals refers to inelastic light scattering by the optical phonons. Within Placzek approximation,[42] the non-resonant Stokes Raman scattering intensities can be computed using the approach developed by Porezag *et al.*[43] and Lazzeri *et al.*[44] The first-order non-resonant Stokes differential Raman cross section for the mth eigenmode can be expressed as[43,45]

$$\frac{d\sigma_m}{d\Omega} = \frac{(2\pi\nu_s)^4}{c^4} |\vec{e}_S \cdot \overleftrightarrow{A}_m \cdot \vec{e}_L|^2 \frac{h(n_m^b + 1)}{8\pi^2 \nu_m}, \tag{6}$$

$$n_m^b = \left[\exp\left(\frac{h\nu_m}{kT}\right) - 1\right]^{-1}, \tag{7}$$

$$A_{m,ij} = \sum_{\tau,p} R_{ij}(\tau p) \frac{U_m(\tau p)}{\sqrt{M_\tau}}, \tag{8}$$

$$R_{ij}(\tau p) = \frac{\Omega}{4\pi} \frac{\partial \varepsilon_{ij}^\infty}{\partial u_{\tau p}}, \tag{9}$$

where ν_S is the frequency of the scattered light, $\vec{e}_S$ and $\vec{e}_L$ are the polarization or unit vectors of the electric-field direction for the scattered and the incident light, n_m^b is the Bose-Einstein statistical factor, $u_{\tau p}$ is the displacement of the τth atom in the p direction, $U_m(\tau p)$ is the orthonormal vibrational eigen-displacement of the mth mode, and M_τ is the mass of atom τ. For single crystals, the Raman intensity can be computed using Eq. (6). However, for polycrystals, the expression for Raman intensity should be appropriately space averaged which depends on the relative orientations of the polarization and direction of the scattered and incident beams. Most Raman scattering experiments involve a plane-polarized incident laser beam wherein direction and the polarization of the incident beam are perpendicular to the direction of observation. For such cases, the Raman cross section can be expressed as

$$\frac{d\sigma_m}{d\Omega} = \frac{2\pi^2(\nu_L - \nu_m)^4}{c^4} \frac{h(n_m^b + 1)}{\nu_m} \frac{I_m^{Act.}}{45}, \tag{10}$$

$$I_m^{Act} = I_{m,||}^{Act} + I_{m,\perp}^{Act}, \tag{11}$$

$$I_{m,||}^{Act} = 45\alpha_m^2 + 4\beta_m^2, \tag{12}$$

$$I_{m,\perp}^{Act} = 3\beta_m^2, \tag{13}$$

where

$$\alpha_m = (A_{m,xx} + A_{m,yy} + A_{m,zz})/3, \tag{14}$$

$$\beta_m^2 = [(A_{m,xx} - A_{m,yy})^2 + (A_{m,xx} - A_{m,zz})^2 + (A_{m,yy} - A_{m,zz})^2 + 6(A_{xy}^2 + A_{yz}^2 + A_{xz}^2)]/2, \tag{15}$$

$$I_m \propto \frac{(n_m^b + 1)}{\nu_m} I_m^{Act}, \tag{16}$$

where I_m and I_m^{Act} are the averaged Raman scattering intensity and Raman activity of the mth mode. $I_{m,||}^{Act}$ and $I_{m,\perp}^{Act}$ are the Raman activities parallel and perpendicular to the incident polarization. Finally, the Raman intensity spectrum can be plotted using the Lorentzian line shape as

$$I(\nu) = \sum_m I_m \frac{\Gamma_m}{(\nu - \nu_m)^2 + \Gamma_m^2}, \tag{17}$$

where Γ_m is the damping coefficient of the mth mode.

The computed relative values of averaged Raman activities and intensities of phonon modes of tetragonal $K_{1/2}Bi_{1/2}TiO_3$ are listed in Table I. As can be seen, Raman activity is significant for modes having frequencies of 230, 335, 355, 523, 527, and 608 cm^{-1}. The mode with a frequency of 608 cm^{-1} exhibits significant IR as well as Raman activity. Further, due to the Bose-Einstein statistical factor and inverse frequency dependence, the modes with frequencies of 66 cm^{-1}, and 121 cm^{-1} exhibit significant relative Raman intensities despite low Raman activities. Figure 7 shows the computed Raman intensity spectrum for $K_{1/2}Bi_{1/2}TiO_3$. As can be seen, strong Raman peaks are centered at modes of 66, 284, 335,
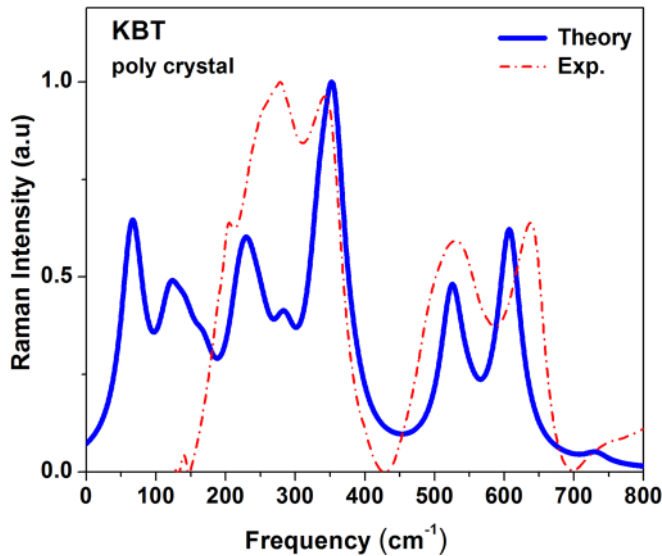
FIG. 7. Computed (solid line) and experimental (dotted line) (Ref. 25) Raman intensity spectra for polycrystalline tetragonal $K_{1/2}Bi_{1/2}TiO_3$.

355, 525, and $607\,cm^{-1}$. The theoretical Raman spectrum is in reasonable agreement with the experimental spectrum which is also shown in Fig. 7.[25] It may be noted that the theoretical Raman spectrum (Fig. 7) is calculated using the $K_{1/2}Bi_{1/2}TiO_3$ unit cell which consists of 10 atoms and has [001] or layered ordering configuration. The Raman intensity spectrum for single crystal tetragonal $K_{1/2}Bi_{1/2}TiO_3$ and for different polarization of incident and scattered beam is shown in Fig. 8.

Next, we study the effect of A-site cation (Bi and K) ordering on the Raman intensity spectrum of tetragonal $K_{1/2}Bi_{1/2}TiO_3$. Figure 9 shows the computed Raman spectrum of $K_{1/2}Bi_{1/2}TiO_3$ with different A-site cation orderings (see Fig. 1). The experimental Raman spectrum is also shown in Fig. 9 for comparison with the theoretical spectrum.[25] As can be seen, the experimental spectrum consists of features which may be attributed to vibrational modes of $K_{1/2}Bi_{1/2}TiO_3$ with different ordering configurations. In particular, two major peaks at $277\,cm^{-1}$ and $345\,cm^{-1}$ in the spectrum clearly indicate the presence of different ordering configurations in the $K_{1/2}Bi_{1/2}TiO_3$ sample. Figure 9 shows that the peak intensity is centered at modes of 276, 275, 263, 278, and $277\,cm^{-1}$ for $K_{1/2}Bi_{1/2}TiO_3$ with [111], [all3 + 1], [10–01$_z$], [11–10$_{xy}$], and [00–01$_z$] ordering configurations, respectively. These computed values are in good agreement with the reported experimental values of $270\,cm^{-1}$,[25] $274\,cm^{-1}$,[9] and $277\,cm^{-1}$.[25] For other ordering configurations in $K_{1/2}Bi_{1/2}TiO_3$ shown in Figs. 1 and 9, the Raman intensity is significantly reduced for these modes. The Raman intensity peak is centered at mode $350\,cm^{-1}$ for $K_{1/2}Bi_{1/2}TiO_3$ with [001] ordering which is in good agreement with the experimental value of $345\,cm^{-1}$ reported in Refs. 24 and 25. In the case of $K_{1/2}Bi_{1/2}TiO_3$ with [100], [110], and [11–01$_{xy}$] orderings, the intensity peak is centered at modes of $333\,cm^{-1}$, $328\,cm^{-1}$, and $320\,cm^{-1}$, respectively. These mode frequency values are more in agreement with the experimental value of $332\,cm^{-1}$ reported in Ref. 9. For $K_{1/2}Bi_{1/2}TiO_3$ with [011]
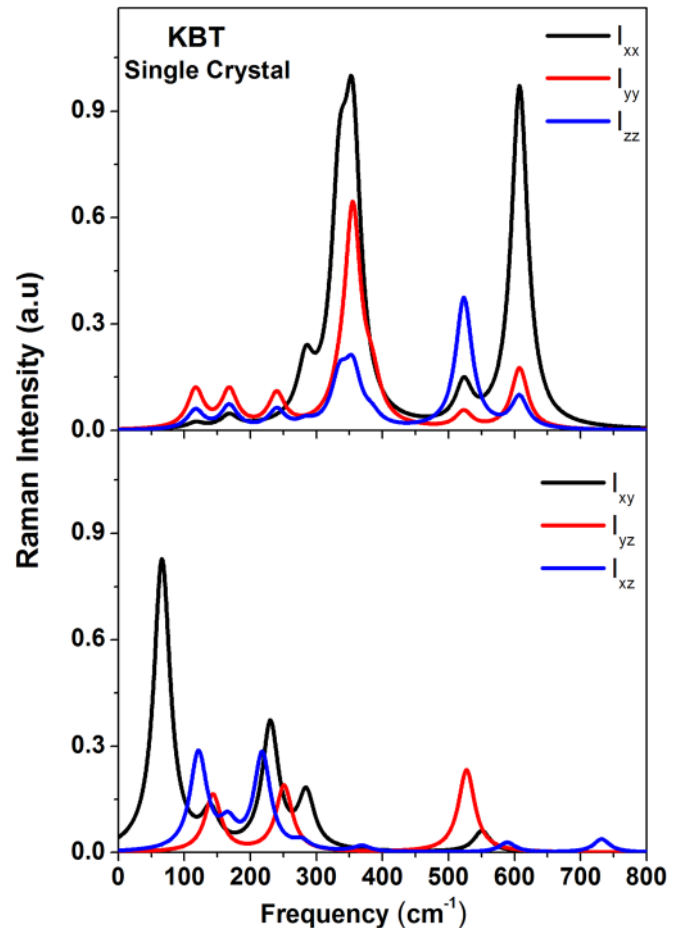

FIG. 8. Computed Raman intensity spectra for single crystal tetragonal $K_{1/2}Bi_{1/2}TiO_3$. The subscript denotes the polarization of incident and scattered beams.

and [100] orderings, the Raman peaks are also centered at $316\,cm^{-1}$ and $362\,cm^{-1}$. In the case of modes with frequencies higher than $400\,cm^{-1}$, the peak is centered at a mode of $495\,cm^{-1}$ in the intensity spectrum of $K_{1/2}Bi_{1/2}TiO_3$ with [100] ordering. This mode frequency is in good agreement with the reported value of $487\,cm^{-1}$ (Ref. 25) and $500\,cm^{-1}$.[24] Further, the peaks are centered at modes of $525\,cm^{-1}$ and $535\,cm^{-1}$ in the intensity spectrum of $K_{1/2}Bi_{1/2}TiO_3$ with [001] and [100] ordering configurations. These mode frequency values are in good agreement with the reported values of $529\,cm^{-1}$ in Ref. 9, $536\,cm^{-1}$ in Ref. 33, and $545\,cm^{-1}$ in Ref. 32. Further, as evident from Fig. 9, the peak positions and the intensities in Raman spectrum are significantly influenced by cation ordering in $K_{1/2}Bi_{1/2}TiO_3$. Moreover, the variance in experimental mode values reported in different studies may be indicative of A-site cation ordering in nanoscale size ordered regions. As discussed in Sec. II B, these ordered nanoregions are expected to be arranged randomly as no single ordering configuration is energetically favorable (see Sec. II B). The random arrangement of nanoscale cation ordered regions is favored by entropy contributions to free energy at finite temperatures. This randomness in arrangement of nanoscale cation ordered regions may explain why long-range A-site cation ordering in $K_{1/2}Bi_{1/2}TiO_3$ has not been observed till
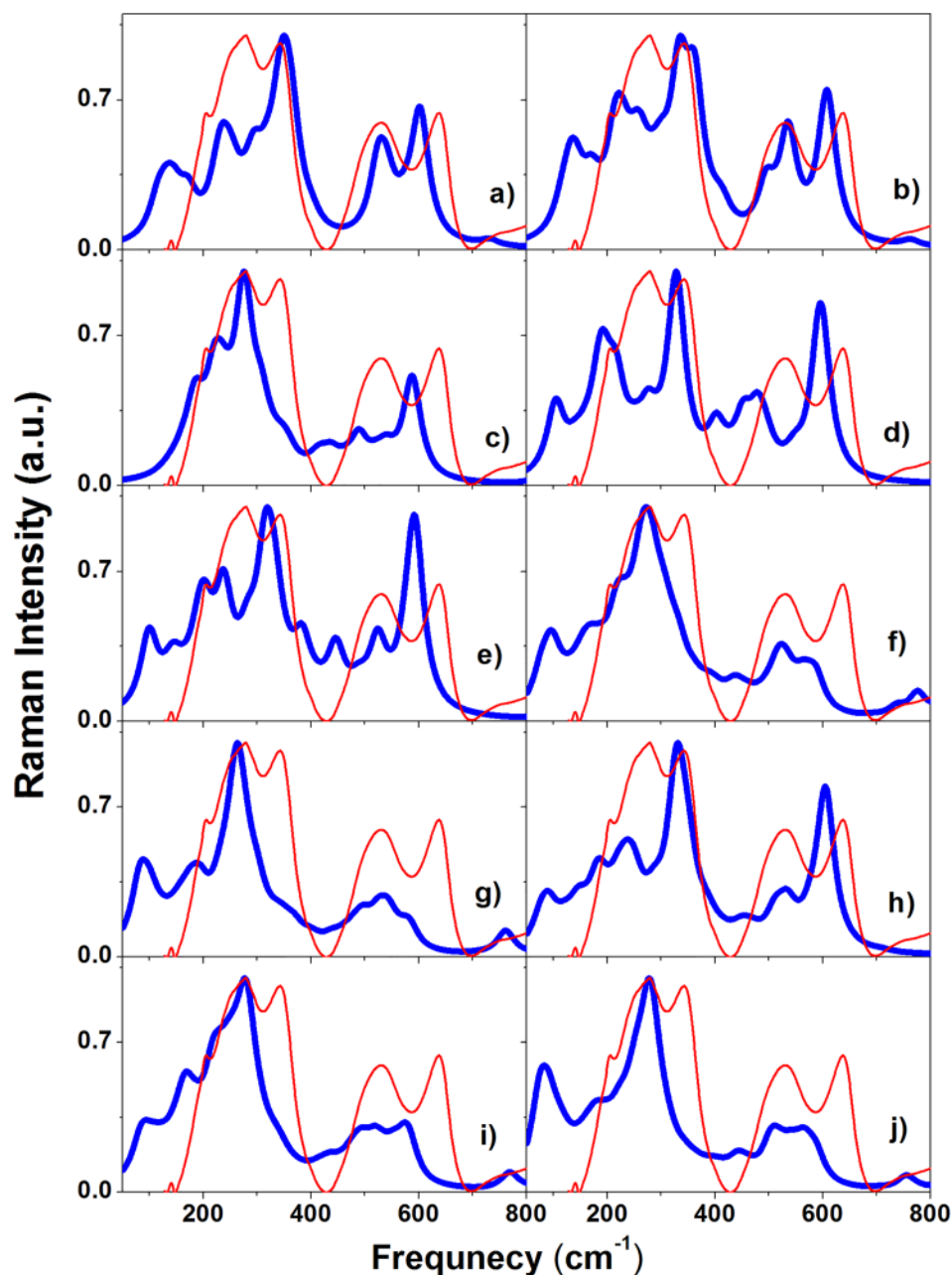
FIG. 9. Computed (solid red line) Raman intensity spectra for different A-site cation orderings in $2 \times 2 \times 2$ tetragonal $K_{1/2}Bi_{1/2}TiO_3$. The types of orderings are (a) [001], (b) [100], (c) [111], (d) [110], (e) [011], (f) [all3 + 1], (g) [10–01$_z$], (h) [11–01$_{xy}$], (i) [11–10$_{xy}$], and (j) [00–01$_z$] (See Fig. 1). The experimental Raman spectrum is shown by a thin red line reported in Ref. 25.

date in diffraction based experiments. Nevertheless, some degree of A-site cation ordering in $K_{1/2}Bi_{1/2}TiO_3$ may still be expected due to kinetic factors which may be dependent on sample preparation conditions. The comparison of theoretical and experimental results suggests that a careful analysis of the Raman intensity spectrum may be exploited to reveal the short range A-site cation ordering in $K_{1/2}Bi_{1/2}TiO_3$.

The suggested formation of A-site cation ordered nanoregions in $K_{1/2}Bi_{1/2}TiO_3$ may have important implications for its relaxor properties similar to that observed in lead based relaxor ferroelectrics of type $A(B'B'')O_3$ such as $Pb(Mg_{1/3}Nb_{2/3})O_3$ (PMN).[26–28] In ergodic relaxor phase of ferroelectrics such as PMN, the polar nanoregions (PNRs) are formed and embedded into the non-polar matrix of the paraelectric phase. In addition to the mixture of polar and nonpolar regions, compositionally (chemical) ordered nanoregions (CORs) are also formed in these relaxor ferroelectrics. However, unlike PNRs, the location, dimensions, and the degree of compositional order inside COR are not dependent on temperature and thereby remain unchanged. It has been suggested that the positions of CORs and PNRs coincide and CORs act as sites to localize the PNRs which emerge below Burns temperature T_B.[27,46] Further, while some reports have suggested that the formation of nanoscale CORs is necessarily required for the appearance of PNRs, others have suggested that dynamics of PNRs is not affected by the morphology of CORs.[26] In the case of $K_{1/2}Bi_{1/2}TiO_3$ too, qualitatively similar CORs with different A-site orderings are expected to form and are likely to be embedded randomly in compositionally disordered matrix (A-site cation disorder). However, partial ordering in arrangement of these CORs may also result due to kinetic factors during sample preparations and besides other experimental probes, a

detailed analysis of Raman spectra may be used to reveal their presence.

III. CONCLUSIONS

Theoretical investigations of lattice dynamics, dielectric and ferroelectric properties, Infrared reflectivity, and Raman intensity spectrum of $K_{1/2}Bi_{1/2}TiO_3$ are performed within the framework of density functional theory. In particular, cation ordering at the A-site in $K_{1/2}Bi_{1/2}TiO_3$ and its effect on lattice dynamics and Raman spectrum are explored. The Raman spectrum is found to be significantly influenced by A-site cation ordering in $K_{1/2}Bi_{1/2}TiO_3$. The comparison of the theoretical Raman spectrum with the experimental spectrum as well as energetics of various ordering configurations of $K_{1/2}Bi_{1/2}TiO_3$ suggests that nanoscale regions with different A-site orderings are formed in $K_{1/2}Bi_{1/2}TiO_3$. However, the arrangement of these ordered nanoregions may be fully or partially random. The layered ordering or [001] configuration of $K_{1/2}Bi_{1/2}TiO_3$ is found to be the lowest energetically and thereby most stable. However, the energies of various other ordering configurations are computed to be only marginally higher (< 40 meV/f.u) than that of the layered ordering configuration. The random arrangement is favored by entropy contributions to free energy and may be accounted for the lack of observation of long-range A-site cation ordering in $K_{1/2}Bi_{1/2}TiO_3$. It is also suggested that kinetic factors during sample preparation may also give rise to partial ordering of cation ordered nanoregions in $K_{1/2}Bi_{1/2}TiO_3$. Further, it is suggested that the Raman spectrum of $K_{1/2}Bi_{1/2}TiO_3$ consists of features which are derived from cation ordered nanoregions with different ordering configurations. The Born effective charges of Bi and Ti ions are found to be significantly larger than their nominal charges. The effective charges of oxygen are found to be quite anisotropic. The disparate Born effective charges of K and Bi ions suggest hetero-polar activity at the A-sites in $K_{1/2}Bi_{1/2}TiO_3$. It is expected that besides PNRs, the formation of A-site hetero-polar cation ordered nanoregions may drive and influence relaxor properties in $K_{1/2}Bi_{1/2}TiO_3$. The oscillator strengths and effective charges of phonon modes are computed. The computed Raman mode frequencies and spontaneous polarization in $K_{1/2}Bi_{1/2}TiO_3$ are found to be in good agreement with the reported experimental values. The Bi-O and Bi-Ti bond distances are found to be in very good agreement with the reported experimental values obtained from XAFS data.

ACKNOWLEDGMENTS

[1]B. Jaffe, W. R. Cook, and H. Jaffe, *Piezoelectric Ceramics* (Academic Press, London, 1971).

[2]A. J. Moulson and J. M. Herbert, *Electroceramics: Materials, Properties and Applications* (John Wiley & Sons Ltd., New York, 2003).

[3]J. Rodel *et al.*, "Perspective on the development of lead-free piezoceramics," J. Am. Ceram. Soc. **92**, 1153 (2009).

[4]Y. Saito *et al.*, "Lead free peizoceramics," Nature **432**, 84 (2004).

[5]E. Cross, "Lead free at last," Nature **432**, 24 (2004).

[6]Y.-M. Chiang *et al.*, "Lead-free high-strain single-crystal piezoelectrics in the alkaline–bismuth–titanate perovskite family," Appl. Phys. Lett. **73**, 3683 (1998).

[7]J. E. Daniels *et al.*, "Electric-field-induced phase transformation at a lead-free morphotropic phase boundary: Case study in a 93%($Bi_{1/2}Na_{1/2}$)TiO_3–7% $BaTiO_3$ piezoelectric ceramic," Appl. Phys. Lett. **95**, 032904 (2009).

[8]V. V. Shvartsman and D. C. Lupascu, "Lead-free relaxor ferroelectrics," J. Am. Ceram. Soc. **95**, 1––26 (2012).

[9]J. F. Yang *et al.*, "Relaxor behavior of ($K_{0.5}Bi_{0.5}$)TiO_3 ceramics derived from molten salt synthesized single-crystalline nanowires," Appl. Phys. Lett. **91**, 023118 (2007).

[10]X. Jing *et al.*, "Structural and electrical properties of $K_{0.5}Bi_{0.5}TiO_3$ thin films for ferroelectric field effect transistor applications," J. Phys. D: Appl. Phys. **42**, 045421 (2009).

[11]Z. F. Li *et al.*, "Dielectric relaxor properties of $K_{0.5}Bi_{0.5}TiO_3$ ferroelectrics prepared by sol–gel method," J. Appl. Phys. **94**, 2548 (2003).

[12]Y. Hiruma *et al.*, "Ferroelectric and piezoelectric properties of ($Bi_{1/2}K_{1/2}$)TiO_3 ceramics. Jpn," J. Appl. Phys. **44**, 5040–5044 (2005).

[13]V. V. Ivanova *et al.*, "X-Ray Determination of the symmetry of elementary cells of the ferroelectric materials $K_{0.5}Bi_{0.5}TiO_3$ and $Na_{0.5}Bi_{0.5}TiO_3$ and of high-temperature phase transitions in $K_{0.5}Bi_{0.5}TiO_3$," Izv. Akad. Nauk SSSR **26**, 354–356 (1962).

[14]G. King and P. M. Woodward, "Cation ordering in perovskites," J. Mater. Chem. **20**, 5785 (2010).

[15]E. Aksel *et al.*, "Local atomic structure deviation from average structure of NBT: Combined X-ray and neutron total scattering study," Phys. Rev. B **87**, 104113 (2013).

[16]M. Gröting, S. Hayn, and K. Albe, "Chemical order and local structure of the lead-freerelaxor ferroelectric," J. Solid State Chem. **184**, 2041––2046 (2011).

[17]M. K. Niranjan *et al.*, "Theoretical and experimental investigation of Raman modes, ferroelectric and dielectric properties of relaxor $Na_{1/2}Bi_{1/2}TiO_3$," J. Appl. Phys. **113**, 194106 (2013).

[18]I. Levin *et al.*, "Local structure, pseudosymmetry, and phase transitions in $Na_{1/2}Bi_{1/2}TiO_3$ -$K_{1/2}Bi_{1/2}TiO_3$ ceramics," Phys. Rev. B **87**, 024113 (2013).

[19]V. A. Shuvaeva *et al.*, "Local structure of the lead-free relaxor ferroelectric (KNa)0.5Bi0.5TiO3," Phys. Rev. B **71**, 174114 (2005).

[20]S. K. Sharma *et al.*, "Raman investigation of ring configurations in vitreous silica," Nature **292**, 140 (1981).

[21]H. Hosono *et al.*, "Physical disorder and optical properties in the vacuum ultraviolet region of amorphous SiO_2," Phys. Rev. Lett. **87**, 175501 (2001).

[22]B. Jiang *et al.*, "Local structure of disordered $Bi_{0.5}K_{0.5}TiO_3$ investigated by pair distribution function analysis and first-principles calculations," Chem. Mater. **29**, 4244 (2017).

[23]M. Groting *et al.*, "Comparative study of A-site order in the lead-free bismuth titanates $M_{1/2}Bi_{1/2}TiO_3$ (M=Li, Na,K,Rb,Cs,Ag,Tl) from first-principles," J. Solid State Chem. **213**, 138–144 (2014).

[24]J. Kreisel *et al.*, "An x-ray diffraction and Raman spectroscopy investigation of A-site substituted perovskite compounds: The $(Na_{1-x}K_x)_{0.5}Bi_{0.5}TiO_3$ ($0 < x < 1$) solid solution," J. Phys.: Condens. Matter **12**, 3267–3280 (2000).

[25]K. Banerjee *et al.*, "Optimum discharge energy density at room temperature in relaxor $K_{1/2}Bi_{1/2}TiO_3$ for green energy harvesting," J. Phys. D: App. Phys. **51**, 115501 (2018).

[26]R. A. Cowley *et al.*, "Relaxing with relaxors: A review of relaxor ferroelectrics," Adv. Phys. **60**(2), 229–327 (2011).

[27]A. A. Bokov *et al.*, "Compositional disorder, polar nanoregions and dipole dynamics in Pb(Mg1/3Nb2/3)O3-based relaxor ferroelectrics," Z. Kristallogr. **226**, 99–107 (2011).

[28]B. P. Burton *et al.*, "Correlations between nanoscale chemical and polar order in relaxor ferroelectrics and the lengthscale for polar nanoregions," Phys. Rev. B **72**, 064113 (2005).

[29]P. Giannozzi *et al.*, J. Phys.: Condens. Matter **21**, 395502 (2009).

[30]N. Troullier and J. L. Martins, "Efficient pseudopotentials for plane-wave calculations," Phys. Rev. B **43**, 1993 (1991).

[31]V. V. Ivanova, A. G. Kapyshev, Y. N. Venetsev, and V. S. Zhdanov, Izv. Akad. Nauk SSSR, Ser. Fiz. **24**, 354 (1962).

[32]M. E. Lines and A. M. Glass, *Principles and Applications of Ferroelectrics and Related Materials* (Oxford University Press, Oxford, 1977).

[33]X. Gonze and C. Lee, "Dynamical matrices, Born effective charges, dielectric permittivity tensors, and interatomic force constants from density-functional perturbation theory," Phys. Rev. B **55**, 10355 (1997).

[34]G.-M. Rignanese, X. Gonze, and A. Pasquarello, Phys. Rev. B **63**, 104305 (2001).

[35]R. D. King-Smith and D. Vanderbilt, Phys. Rev. B **47**, 1651 (1993).

[36]P. V. B. Rao *et al.*, "Impedance spectroscopy studies of $K_{0.5}Bi_{0.5}TiO_3$," J. Electroceram. **25**, 60–69 (2010).

[37]J. Konig and D. Suvorov, "Evolution of the electrical properties of $K_{0.5}Bi_{0.5}TiO_3$ as a result of prolonged sintering," J. Eur. Ceram. Soc. **35**, 2791 (2015).

[38]X. Gonze, P. Ghosez, and R. W. Godby, "Density-polarization functional theory of the response of a periodic insulating solid to an electric field," Phys. Rev. Lett. **74**, 4035 (1995).

[39]S. Baroni and R. Resta, "*Ab-initio* calculation of the macroscopic dielectric constant in silicon," Phys. Rev. B **33**, 7017 (1986).

[40]R. Resta, "Local-field effects and phonon screening in polar semiconductors," Phys. Rev. B **27**, 3620 (1983).

[41]V. Zelezny, E. Cockayne, J. Petzelt, M. F. Limonov, D. E. Usvyat *et al.*, "Temperature dependence of infrared-active phonons in CaTiO3: A combined spectroscopic and first-principles study," Phys. Rev. B **66**, 224303 (2002).

[42]P. Bruesch, *Phonons: Theory and Experiments II* (Springer, Berlin, 1986).

[43]D. Porezag *et al.*, "Infrared intensities and Raman-scattering activities within density-functional theory," Phys. Rev. B **54**, 7830 (1996).

[44]M. Lazzeri *et al.*, "First-principles calculation of vibrational Raman spectra in large systems: Signature of small rings in crystalline SiO_2," Phys. Rev. Lett. **90**, 036401 (2003).

[45]M. Cardona *et al.*, *Light Scattering in Solids* (Springer-verlag, Berlin, 1982), vol. 50.

[46]L. E. Cross, "Relaxor ferroelectrics: An overview," Ferroelectrics **151**, 305–320 (1994).